

THE TYPE II SUPERNOVA RATE IN $z \sim 0.1$ GALAXY CLUSTERS FROM THE MULTI-EPOCH NEARBY CLUSTER SURVEY

M. L. GRAHAM^{1,2}, D. J. SAND^{1,2,3}, C. J. BILDFELL⁴, C. J. PRITCHET⁴, D. ZARITSKY⁵, H. HOEKSTRA⁶, D. W. JUST⁵, S. HERBERT-FORT⁵, S. SIVANANDAM⁷, R. J. FOLEY^{8,9}

To appear in ApJ., XX.

ABSTRACT

We present 7 spectroscopically confirmed Type II cluster supernovae (SNeII) discovered in the Multi-Epoch Nearby Cluster Survey, a supernova survey targeting 57 low redshift $0.05 < z < 0.15$ galaxy clusters with the Canada-France-Hawaii Telescope. We find the rate of Type II supernovae within R_{200} of $z \sim 0.1$ galaxy clusters to be $0.026_{-0.018}^{+0.085}(\text{stat})_{-0.001}^{+0.003}(\text{sys})$ SNU_M. Surprisingly, one SNII is in a red sequence host galaxy that shows no clear evidence of recent star formation. This is unambiguous evidence in support of ongoing, low-level star formation in at least some cluster elliptical galaxies, and illustrates that galaxies that appear to be quiescent cannot be assumed to host only Type Ia SNe. Based on this single SNII we make the first measurement of the SNII rate in red sequence galaxies, and find it to be $0.007_{-0.007}^{+0.014}(\text{stat})_{-0.001}^{+0.009}(\text{sys})$ SNU_M. We also make the first derivation of cluster specific star formation rates (sSFR) from cluster SNII rates. We find that for all galaxy types, the sSFR is $5.1_{-3.1}^{+15.8}(\text{stat}) \pm 0.9(\text{sys}) M_{\odot} \text{ yr}^{-1} (10^{12} M_{\odot})^{-1}$, and for red sequence galaxies only, it is $2.0_{-0.9}^{+4.2}(\text{stat}) \pm 0.4(\text{sys}) M_{\odot} \text{ yr}^{-1} (10^{12} M_{\odot})^{-1}$. These values agree with SFRs measured from infrared and ultraviolet photometry, and H α emission from optical spectroscopy. Additionally, we use the SFR derived from our SNII rate to show that although a small fraction of cluster Type Ia SNe may originate in the young stellar population and experience a short delay time, these results do not preclude the use of cluster SNIa rates to derive the late-time delay time distribution for SNe Ia.

Subject headings: supernovae: general — galaxies: clusters

1. INTRODUCTION

The rates and properties of Type II supernovae (SNeII) indicate they are explosions induced by the collapse of iron cores in stars of initial masses $8 < M \lesssim 20 M_{\odot}$ (Smartt et al. 2009). Such massive progenitors have been directly confirmed in pre-explosion images for several SNeII (Li et al. 2007a; Gal-Yam et al. 2007; Smartt et al. 2009; Elias-Rosa et al. 2011; Maund et al. 2011). Stars of initial mass $> 8 M_{\odot}$ explode as SNe with a delay time, the time between star formation and explosion, of $\lesssim 30$ Myr (e.g. Henyey et al. 1959). Due to this relatively short delay time the SNII rate, SNR_{II} , is a direct indication of the current star formation rate, SFR (Botticella et al. 2012). Since SNeII are bright, using SNR_{II} to identify very low levels of star formation (SF) can be advantageous to using ultraviolet (UV) photometry or optical spectroscopy. For example, small amounts of UV light may be undetectable in a luminous ellipti-

cal, and a little H α emission in an elliptical can be overwhelmed by an active galactic nucleus. Also, at low redshift UV photometry can be an ambiguous SF tracer because of contributions from blue horizontal branch stars (the UV upturn). The SNR_{II} is thus an especially valuable SFR proxy in rich galaxy clusters, which are mainly composed of luminous elliptical galaxies.

Evidence for low levels of SF has recently been detected in low redshift cluster galaxies from optical spectra (Fritz et al. 2011) and infrared photometry (Chung et al. 2011), and in low redshift field red sequence galaxies from UV photometry (Kaviraj et al. 2010). Despite this, SNeII have rarely been observed in early-type galaxies where the bulk of the stellar mass is in old stellar populations (Hakobyan et al. 2008). As a result, the SNR_{II} in field ellipticals and cluster galaxies is not well constrained. Table 1 presents the current literature values for SNR_{II} . The Lick Observatory Supernova Search (LOSS; Leaman et al. 2011) placed an upper limit on SNR_{II} in field ellipticals, and provided the first measurement of SNR_{II} in field S0 galaxies (Li et al. 2011b). Five SN surveys were combined by Mannucci et al. (2008; hereafter M08), who measured the SNR_{II} in galaxy clusters to be half the rate in field galaxies, but well above the upper limits of field ellipticals. However, the surveys compiled by M08 were biased towards the most massive cluster members, and their SNe were not all spectroscopically classified. In this paper we present the SNR_{II} measurement from our large, complete, well characterized cluster SN survey at low redshifts, and make the first comparison of SNII-derived cluster SFR to the recently detected low levels of SF from optical, IR, and UV data.

¹ Las Cumbres Observatory Global Telescope Network, 6740 Cortona Drive, Suite 102, Santa Barbara, CA 93117, USA

² Department of Physics, Broida Hall, University of California, Santa Barbara, CA 93106, USA

³ Harvard Center for Astrophysics and Las Cumbres Observatory Global Telescope Network Fellow

⁴ Department of Physics and Astronomy, University of Victoria, PO Box 3055, STN CSC, Victoria BC V8W 3P6, Canada

⁵ Steward Observatory, University of Arizona, Tucson AZ 85721

⁶ Leiden Observatory, Leiden University, Niels Bohrweg 2, NL-2333 CA Leiden, The Netherlands

⁷ Dunlap Fellow, Dunlap Institute for Astronomy and Astrophysics, 50 St. George St., Toronto, ON Canada M5S 3H4

⁸ Harvard-Smithsonian Center for Astrophysics, 60 Garden Street, Cambridge, MA 02138, USA

⁹ Clay Fellow.

In contrast to SNeII, SNeIa occur in both young and old stellar populations (Mannucci et al. 2005; Scannapieco & Bildsten 2005). Ongoing star formation in galaxy clusters is a concern when using the cluster SNR_{Ia} to constrain the slope of the SNIa delay time distribution (DTD). The two leading scenarios for the SNIa progenitor are a carbon-oxygen white dwarf accreting material from a main sequence or red giant star (single degenerate), or accreting from or merging with another white dwarf (double degenerate). Each occur over different timescales and predict distinctive DTDs at late times; i.e. the double degenerate scenario predicts more delayed SNeIa. The colors of cluster red sequence galaxies indicate that their star formation was truncated at high redshift, and they have evolved passively since (e.g. Stanford et al. 1998; Eisenhardt et al. 2008). Based on this, it is assumed that cluster SNeIa have all experienced long delay times, and that the cluster $SNR_{Ia}(z)$ can constrain the late-time DTD (i.e. Maoz et al. 2010). However, the presence of ongoing star formation suggests the cluster population may be contaminated by short-delay SNeIa. In this paper we use our SNIa-derived cluster SFR to evaluate this possibility.

The Multi-Epoch Nearby Cluster Survey (MENeACS) surveyed 57 low redshift $0.05 < z < 0.15$ galaxy clusters for two years with the Canada-France-Hawaii Telescope (CFHT). Within the virial radius, R_{200} , of our cluster sample, we spectroscopically classified 7 cluster SNeII and 23 cluster Type Ia supernovae. This paper is part of a series based on MENeACS. In Sand et al. (2011; hereafter S11) we use the relative number of hosted and hostless SNeIa to determine the mass fraction of intracluster stars. In Sand et al. (2012; hereafter S12), we measure the cluster SNR_{Ia} from MENeACS, and combine it with published SNIa rates between $0.02 < z < 1.12$ to constrain the slope of the SNIa delay-time distribution. Two additional MENeACS papers are nearing publication: one showing evolution in the cluster dwarf-to-giant galaxy ratio over redshift (Bildfell et al. 2012), and one investigating the demographics of tidally disturbed galaxies in clusters (Adams et al. in preparation).

In this work we present the 7 cluster SNeII, including the unprecedented occurrence of a SN II in a red sequence galaxy. In § 2 we describe MENeACS, and present the photometric and spectroscopic properties of our 7 cluster SNeII and their hosts galaxies, including a comparison of SN II and SNIa hosts. In § 3 we constrain the level of ongoing star formation in our one red sequence SN II host galaxy using published multi-wavelength data. In § 4 we describe our SN II rate calculation and its uncertainties, and compare our results to published rates. In § 5 we derive the star formation rate in clusters, and compare it to measurements from IR, UV, and spectroscopic observations of cluster galaxies. We also discuss the implications for the SNIa DTD. We provide a summary of this paper in § 6, and in all cases we use a standard flat cosmology of $(\Omega_M, \Omega_\Lambda) = (0.3, 0.7)$ and $h = 0.7$.

2. THE MENEACS SN II SAMPLE

MENeACS monitored 57 rich galaxy clusters with monthly cadence for two years in the g' - and r' -band filters with MegaCam (Boulade et al. 2003) at the CFHT. The survey design, cluster sample, observing strategy, real-time reductions, transient detection pipeline, photo-

metric calibration, host identification, and spectroscopic SN classification techniques we used to discover supernovae are presented in S12. The data were reduced and searched for transients in real time, with regular spectroscopic runs scheduled each month of the survey for supernova classification with the Blue Channel Spectrograph (BCS; Schmidt et al. 1989) or Hectospec (Fabricant et al. 2005) at the MMT Observatory. Photometric calibrations to SDSS filters g and r in the AB magnitude system were performed using standard stars in the fields.

We spectroscopically followed up all SN candidates brighter than $m_g=22.5$ magnitudes, and with colors $g - r > 0.8$. As described in S12, we used the publicly available Supernova Identification (SNID) routine of Blondin & Tonry (2007) to spectroscopically classify our SNe. Cluster membership was assigned for SNe with $|v_{SN} - v_{cluster}| < 3000 \text{ km s}^{-1}$. In total we confirmed 23 SNeIa (4 of which were hostless), 7 SNeII associated with our clusters, and 37 background SNe. Due to the one square degree field of view of MegaCam, we are complete to $\sim R_{200}$ and can calculate SN rates within this radius. For comparison with past surveys, we also present rates within $R = 1 \text{ Mpc}$.

Table 2 presents the 7 SNeII discovered in MENeACS clusters including their internal identification name; the UT date of spectroscopy; the telescope and instrument for follow-up; cluster redshift; galaxy redshift where available; details of the SNID best fit including redshift (and uncertainty), SN template type and name, and median phase (and the standard deviation); and finally the spectroscopic exposure time in seconds. Figure 1 presents the classification spectra for each; all 7 are best fit with Type II plateau spectral templates.

As discussed by Li et al. (2011a), reliable distinction between Type II subtypes requires multiple spectra *and* well sampled light curves. Type IIn (narrow spectral lines) are spectrally distinctive but can evolve to resemble a regular Type II. The Type IIL are spectroscopically similar to Type IIP, but have a linearly declining light curve and no plateau phase. Type IIb (broad spectral lines) can resemble normal Type II at early times, but their light curves are distinctly double-peaked. With the single epoch of spectroscopy and monthly photometric cadence of MENeACS, we cannot confidently identify subtypes for our SNeII.

2.1. MENeACS SN II Host Galaxies

Photometry for MENeACS SN II host galaxies is measured from SN-free deep stack images, as described in S12. Table 3 presents the host galaxy details for each cluster SN II, including the coordinates, r -band magnitude, $g - r$ color, the $\Delta(g - r)_{RS}$ color offset from the cluster's red sequence, and the clustercentric radius in units of kiloparsecs and R_{200} . Clustercentric radius is the distance from the brightest cluster galaxy (BCG); for our 7 SNeII host clusters the BCGs are within $30''$ of the X-ray centers (from Chandra and ROSAT), except for Abell 2443 which has a $\sim 1.5'$ offset. However, even a potential $1.5'$ shift could not cause any SNeII to cross the R_{200} boundary, and be included or excluded from the sample.

Given that SN II progenitors are young, but SNeIa occur in both young and old stellar populations, we expect the distributions of $g - r$ colors to be different for

SN II and SN Ia host galaxies. In Figure 2 we plot the $\Delta(g-r)_{RS}$ color offset from the cluster red sequence as a function of r -band magnitude for SN Ia and SN II hosts. The dashed lines represent the median scatter in the red sequence for the MENeCS sample. All host galaxies with $\Delta(g-r)_{RS}$ error bars overlapping this zone are considered to lie “on” the red sequence, and all others lie “off” the red sequence. Unlike the SNe Ia host population, SN II hosts lie off their clusters’ red sequences – except for the host SN II Abell399_11_19_0, discussed in § 3. In Figure 3, we show that the distributions of host $g-r$ colors are significantly different for SNe Ia and SNe II. The KS-test probability that the two samples are drawn from the same underlying distribution is low, but not negligible, at $\sim 8\%$.

Chung et al. (2011) show that the fraction of star forming galaxies increases with projected clustercentric radius within R_{200} . We therefore expect the radial distribution of SN II hosts to differ from SN Ia hosts, which should in turn follow the cluster luminosity profile. In Figure 2 we plot the $\Delta(g-r)_{RS}$ color offset from the cluster red sequence as a function of projected clustercentric radius, for both SN Ia and SN II hosts. We note that no off-RS MENeCS hosts are observed within $0.3 R_{200}$, consistent with the view that the star formation fraction decreases in the central regions of clusters (Chung et al. 2011). Figure 3 shows the distributions of projected clustercentric radii for SN Ia and SN II hosts. The normalized, cumulative fraction of cluster g -band luminosity in red sequence galaxies is also plotted. Within R_{200} it appears the number of SNe is roughly proportional to luminosity.

3. THE RED SEQUENCE SN II HOST

Unexpectedly, one of our seven MENeCS SNe II occurred in a red sequence galaxy. As we discuss below, based on its spectrum and photometry we are confident that it was a SN II and not a SN Ia. The color, magnitude, red sequence offset, and clustercentric distance for the host galaxy of Abell399_11_19_0 are listed in Table 3, and are shown to be consistent with the red sequence in Figure 2. In Figure 4 we show an image of this galaxy with isophotal contours to highlight this galaxy’s elliptical morphology.

When core collapse SN (CCSNe, Types II and Ibc) are discovered in elliptical galaxies, further inspection almost always reveals the presence of star formation. Hakobyan et al. (2008) appraised 22 elliptical galaxies hosting CCSNe; of them, 19 were misclassified as elliptical, and three showed evidence of mergers or interactions and were thus likely to harbor recent star formation. Suh et al. (2011) investigated the near-ultraviolet and radio properties of nine early-type CC SN hosts, finding clear evidence of recent star formation in all. These results are consistent with the relative youth of SN II progenitor stars. In this section we look for evidence of recent star formation in the UV, IR, spectral, and radio properties of the host of Abell399_11_19_0.

3.1. SN Classification

The classification spectrum taken for Abell399_11_19_0 with Hectospec at the MMT Observatory is shown in Figure 1, along with the best fitting SN template spectrum from SNID (Blondin & Tonry 2007). The P-Cygni profile, distinctive for SN II, appears at $\sim 7000 \text{ \AA}$. Since

the fit with SNID may not be overwhelmingly convincing for all our readers, we do an additional analysis with Superfit (Howell et al. 2005). This routine achieves a better looking fit because it removes the host galaxy spectrum. First we run Superfit with loose redshift constraints, $0.05 < z < 0.25$, to independently confirm the SN redshift. We know the host’s spectroscopic redshift is $z = 0.072$, and the SN-host association is unambiguous (Figure 4). The top 3 best fits are SNe II at $z = 0.07$. We then run Superfit two additional times with the redshift constrained to $z = 0.07$: first allowing only SN II templates, then SN Ia only. The best fits, in Figure 5, show that a SN II is the better match.

The MENeCS cadence of one epoch per month did not generate well sampled light curves, but given the relative importance of Abell399_11_19_0 we discuss its photometry briefly. Following a non-detection epoch in October 2009, this transient was detected in three consecutive months, after which the MENeCS observations ended. This transient had $m_g \sim m_r \sim 20$ magnitudes in the detection epoch (corresponding to $M \sim -17.5$ magnitudes). In ~ 55 days it declined by $\Delta m_g \sim 2$ magnitudes and $\Delta m_r \sim 1$ magnitude. When compared to the light curve templates of Nugent et al. (2002) and SN luminosity functions of Li et al. (2011a), this color, magnitude, and slow decline are all most consistent with a SN II Plateau. Regular SNe Ia are too bright, and faint SNe Ia decline too quickly (Phillips 1993; Perlmutter et al. 1997). Finally, the preceding non-detection epoch prohibits this from being the late-time shallow-decline epochs of a SN Ia.

3.2. Ultraviolet Photometry

If this host galaxy experienced a small amount of recent star formation, it might be evident in its near-ultraviolet photometry. Schawinski (2009) generate model spectra from near ultraviolet (NUV) to optical wavelengths by parametrizing the star formation history of early-type galaxies as a large population of old stars plus a small amount of young stars. They show how a galaxy’s $NUV-r$ color indicates the time elapsed since the most recent burst of star formation, given the fraction of stellar mass synthesized in the burst. For example, in an early-type galaxy where $\sim 1\%$ of the stellar mass is $\lesssim 50$ Myr old, $NUV-r \lesssim 1$. Similarly, Kaviraj (2010) use star formation history models to derive a relationship between the UV and optical photometry of bulge-dominated red galaxies, and the age and mass fraction of their most recent epoch of SF.

We look for the UV counterpart of this host in the GALEX data release 6¹⁰. There is no coincident object in the catalog, and under visual inspection the tiles show no hint of a source. From Bianchi et al. (2011), we know that UV sources are detected at 5σ down to $NUV \sim 20.8$ magnitudes in the GALEX All-sky Imaging Survey, and that the Medium-depth Imaging Survey does not cover this region of sky. With this limit, we restrict the $NUV-r$ color to > 4.5 . Based on Schawinski (2009), this constrains the fraction of stars < 50 Myr old to $\ll 1\%$ of the total stellar mass of this SN II host galaxy. Comparably, the work presented in Kaviraj

¹⁰ <http://galex.stsci.edu/GR6/>

(2010) constrains the age and mass fraction of the most recent burst to $\gtrsim 250$ Myr and $< 0.5\%$, respectively.

3.3. Infrared Photometry

Photometry at optical and near-infrared (NIR) wavelengths can be combined to reveal recent star formation in an evolved galaxy. Stellar population synthesis models have been used by Li et al. (2007) to determine that $B - V$ and $B - K$ photometric colors best disentangle the degeneracy between galaxy age and metallicity. They show that a galaxy’s location on a $B - V$ vs. $B - K$ color-color plot can be used to estimate the fraction of mass in young stars. To obtain these colors for this host we begin with our photometry, $m_g = 17.1 \pm 0.02$ magnitudes and color $g - r = 0.85 \pm 0.04$, and add 2MASS $m_K = 13.62 \pm 0.18$ magnitudes (from NASA Extragalactic Database). We then K-correct to $z = 0$ (Chilingarian et al. 2010), and apply filter transformations derived for stars at $z = 0$ (Jester et al. 2005), to obtain $B - V = 0.9 \pm 0.04$ and $B - K = 3.6 \pm 0.2$. These colors suggest $\lesssim 0.5\%$ of the stellar mass is younger than 0.5 Gyr (Li et al. 2007b).

Galaxies which appear quiescent from optical and NIR photometry can harbor dust-obscured star formation, and be luminous at far-infrared (FIR) wavelengths. In this scenario, dust absorbs UV light and re-emits it in the FIR. Chary & Elbaz (2001) present conversions from the Spitzer-MIPS 24 μm wavebands to infrared luminosity, L_{IR} , and star formation rates, SFR_{IR} . For example, Graham et al. (2010) applied these conversions to Spitzer-MIPS fluxes for 20 optically elliptical SNIa host galaxies from the Supernova Legacy Survey, and found 2 were actually Luminous Infrared Galaxies (LIRGs, $L_{IR} > 10^{11} L_{\odot}$) with specific star formation rates $\sim 500 M_{\odot} \text{ yr}^{-1} (10^{12} M_{\odot})^{-1}$.

This red sequence host was observed by the Wide-field Infrared Survey Explorer (WISE; Wright et al. 2010) in its mission to create an all-sky infrared map, and the WISE-W4 filter at 22 μm compares well with Spitzer MIPS 24 μm^{11} . In W4, this galaxy has an apparent magnitude of 15.2 in the AB system (8.6 in the Vega system), but a signal-to-noise ratio of just 1.4 and a $\sigma = \text{null}$, indicating this magnitude is a 95% confidence upper limit. We convert this magnitude limit to a flux and find $L_{IR} < 10^9 L_{\odot}$. This is not a LIRG masquerading as a quiescent elliptical.

3.4. Optical Spectroscopy

We obtained an optical spectrum of this galaxy with the Blue Channel Spectrograph at the MMT Observatory as part of our program to gather spectra for all our SNeIa cluster hosts. Full spectral analyses will be performed for all of our SN cluster host galaxies in future work (Graham et al. 2012, in preparation).

The partial spectrum presented in Figure 4 reveals hydrogen emission, indicative of star formation – but also shows the nitrogen, oxygen, and sulfur signatures of a low-ionization nuclear emission-line region (LINER). Kewley et al. (2006) show that star formation is not the dominant source of emission when $\log([NII]/H\alpha) > 0.0$ and $\log([SII]/H\alpha) > 0.0$. A simple analysis of this galaxy’s line intensities finds that [NII]

and [SII] are stronger than $H\alpha$ ($\log([NII]/H\alpha) \sim 1.1$ and $\log([SII]/H\alpha) \sim 0.6$). We estimate the maximum amount of $H\alpha$ absorption by fitting template spectra of elliptical galaxies (Kinney et al. (1996); Fioc & Rocca-Volmerange 1997). After accounting for the template fit with the largest absorption, we are confident that the line intensity of $H\alpha$ is < 4 . This indicates the minimum line ratio values are $\log([NII]/H\alpha) > 0.4$ and $\log([SII]/H\alpha) \gtrsim 0.0$, which is still consistent with a LINER. While these spectral emission lines mean we cannot attribute the $H\alpha$ to SF, we also cannot rule it out. The slit did cross the galaxy core, and future observations with a slit orientation avoiding the core may reveal SF at this SN’s location.

3.5. Radio Power

Radio-loud emission ($L_{1.4\text{GHz}} > 10^{29} \text{ erg s}^{-1} \text{ Hz}^{-1}$) from elliptical galaxies could indirectly represent ongoing star formation (e.g. Della Valle et al. 2005). We checked published radio source catalogs for 1.4 GHz emission at this galaxy’s position. Its coordinates are not covered by the VLA FIRST Survey¹², and it was not detected in the NRAO VLA Sky Survey¹³ (NVSS). The completeness limit of the NVSS at 1.4 GHz is 2.5 mJy. At the redshift of this host, $z = 0.072$, the radio-loud population is incomplete and we cannot constrain the radio properties of this host.

In summary we find no evidence of star formation in this galaxy, aside from the presence of the SNIa. This indicates that either very low levels of star formation and trace amounts of young stellar populations can exist in red sequence galaxies, or there is a rare other channel to SNeII with a longer delay time.

4. THE CLUSTER SNIa RATE

Our calculation of the SNIa rate in clusters follows the method we used for SNIa rates in S12, which is very similar to that used for high and low redshift SN rates by Sharon et al. (2007) and Barbary et al. (2012). The rate of Type II supernova, SNR_{II} , is calculated by:

$$SNR_{II} = \frac{N_{II} \times C_{inc}/C_{spec}}{\sum_{j=1}^{j=N_{ep}} \Delta t_j M_j}, \quad (1)$$

where N_{II} is the observed number of SNeII. The spectroscopic completeness, $C_{spec} = 0.91$, accounts for the $\sim 9\%$ of the time when MENeACS was detecting SNe, but we did not have spectroscopic follow-up due to weather and telescope scheduling. This value is independent of SN type (see S11 and S12). The inclination correction, C_{inc} , accounts for SNeII that are undetectable due to extreme dust obscuration in highly inclined and edge-on spiral galaxies (e.g. Cappellaro et al. 1993b; Cappellaro et al. 1999); our inclination correction, $C_{inc} = 1.62$, is derived in Appendix A. Over all N_{ep} survey epochs of every cluster we sum the control time for that epoch, Δt_j , multiplied by the mass or luminosity surveyed in that epoch, M_j (see S12 for a description of how these are calculated from our deep image stacks).

The control time is the effective amount of time surveyed by the j^{th} epoch, expressed by:

¹² <http://sundog.stsci.edu/>
¹³ <http://www.cv.nrao.edu/nvss/>

¹¹ Supplement at <http://wise2.ipac.caltech.edu/docs/release/prelim>

$$\Delta t = \int_{t_1}^{t_2} \eta(m(t)) dt, \quad (2)$$

where $\eta(m)$, the MENEaCS detection efficiency as a function of apparent magnitude, is determined from simulated transients and is presented in S12. Although the population of simulated transients used for our recovery statistics have magnitude distributions that mimic a sample of SNe Ia, the resulting detection efficiency is appropriate for use with our SNe II. For the SN II light curve, $m(t)$, we start with the absolute V -band SN II template light curves from Nugent et al. (2002). MENEaCS detection efficiencies were calculated in the g -band. We convert from M_V to m_g using the cluster's redshift, the SN II K-correction (based on spectral templates from Nugent et al. 2002), and the photometric calibrations for the j^{th} epoch. The integration boundaries t_1 and t_2 are defined by the time during which the SN II template light curve meets our color limit for spectroscopic follow-up, $g-r < 0.8$ (e.g. 39 days for $z = 0.15$, and 66 days for $z = 0.05$). We account for potential rediscovers of the same transient in multiple epochs by subtracting from $\eta(m)$ the probability that it was detected previously, in the same fashion as S12 and Sharon et al. (2007).

We use a Monte Carlo method in which the rate is calculated many times. For each realization a peak absolute magnitude is randomly chosen from the luminosity function discussed in § 4.1. At every instance of M_j , $\eta(m)$, and N_{II} , we randomly draw their value from an appropriate distribution based on their uncertainty (e.g. Poisson error for N_{II}). We run this Monte Carlo calculation for 500 realizations, which generates a distribution of rates. The final value for the rate is the median of this distribution, and the statistical uncertainties correspond to the 16th and 84th percentiles (the 68% confidence interval). The final results are presented in § 4.3.

4.1. The SN II Luminosity Function

For each realization of the Monte Carlo we randomly draw the SN II subtype (P, L, b, or n) and peak absolute magnitude from the volume-limited luminosity functions (LFs) published by the LOSS (Li et al. 2011a; hereafter Li11a). We use their LFs for type S0-Sbc hosts because the majority of the stellar mass in cluster environments is in early-type galaxies. The fractions of each SN II subtype in S0bc host galaxies are: P, 72%; L, 12%; b, 9%; and n, 7%. These fractions do not change by more than 2% when all host types are considered, and the SN II LF for all host types is very similar to that for S0bc only. We also use the appropriate light curve template for each subtype from Nugent et al. (2002); the SN IIL light curve when subtype L is chosen, and the SN IIP light curve when subtypes P, b, or n are chosen.

To compare to the SNR_{II} from M08, we repeat the Monte Carlo process using the same SN II LF as them: that of Cappellaro et al. (1993a; hereafter C93a). They present the SN II LF as Gaussian functions for subtypes P and L separately: peak $M_{B,IIP} = -16.38$, $\sigma_{IIP} = 1.49$, peak $M_{B,IIL} = -16.82$, and $\sigma_{IIL} = 1.1$ magnitudes. In Figure 6 we compare the SN II LFs from Li11a and C93a. To plot a single LF from C93a, we combine the IIP and IIL into one Gaussian of peak

$M_B = -16.51$ magnitudes, $\sigma = 1.85$ magnitudes, assuming 30% SN IIL and 70% SN IIP. As is evident in Figure 6, Li11a detects a population of faint SN II-P ($M_B \sim -14$ magnitudes), which results in a non-Gaussian LF. However, since MENEaCS is not sensitive to transients fainter than $M_B \sim -14.6$ magnitudes, these two LFs produce effectively similar results. This is discussed further in § 4.4.

Here we make two important notes about how we incorporate the SN II LFs and light curves. First, the Li11a distribution of absolute peak magnitudes from their unfiltered survey is very closely matched to R-band, and can be considered as M_R magnitudes with no correction. The C93a LF is for M_B , which peaks several days earlier, and the Nugent et al. (2002) light curve templates are for M_V . Fortunately, we do not need to convert between filters because the intrinsic $B-V$ and $V-R$ colors of SNe II at the time of B - and V -band maximum light is ~ 0 (e.g. Poznanski et al. 2002; d'Andrea et al. 2010). Although SNe II will be redder a few days later, at the time of maximum light in the R -band this is due to a decline in B and V ; the R -band magnitude increases only slightly between the times of B - and R -band maximum light. Therefore, we directly apply the R -band LF of Li11a and the B -band LF of C93a to the V -band light curve templates of Nugent et al. (2002).

Second, neither Li11a nor C93a correct their SN II LFs for host extinction, and by choosing randomly from these LFs we automatically include host extinction in our Monte Carlo rate calculation. By using the Li11a LF for S0-Sbc type hosts, the host extinctions are as similar to that expected for cluster galaxies as possible because most cluster galaxies are of similar early types. While the observed colors of SNe II-P do have a spread due to host reddening (e.g. Hamuy 2003; Krisciunas et al. 2009; Olivares E. et al. 2010), this affect is expected to be small for most of our surveyed mass in galaxy clusters. For example, Hamuy (2003) find that SNe II associated with groups/clusters show little to no reddening. The affect of host reddening and extinction on SNR_{II} is accounted for by the combination of our chosen LFs because they are uncorrected for host dust, and by our inclination correction which is discussed below.

4.2. Interlopers

As mentioned in § 2, cluster membership was assigned for SNe with $|v_{SN} - v_{cluster}| < 3000$ km s $^{-1}$, which actually includes ~ 50 Mpc in front of and behind each cluster. Any SNe II exploding in Hubble flow galaxies within this cylindrical volume may be erroneously associated with our galaxy clusters. The number of interlopers we expect to have observed, N_{exp} , after accounting for our detection efficiencies is:

$$N_{exp} = \frac{R_{vol} C_{spec}}{C_{inc}} \sum_{j=1}^{j=N_{ep}} \Delta t_j V_j. \quad (3)$$

The volumetric SN II rate at $z \sim 0.1$ is $R_{vol} \sim 7 \pm 3 \times 10^{-5}$ SN yr $^{-1}$ Mpc $^{-3}$ (Bazin et al. 2009). The MENEaCS spectroscopic completeness term $C_{spec} = 0.91$. The inclination correction, C_{inc} , is discussed in Appendix A. We assume an interloper-hosting field galaxy would not be elliptical, which slightly raises the inclination correc-

tion factor used here to $C_{inc} = 1.72$. The final term is the control time, Δt , multiplied by V_j , the comoving volume element within $\pm 3000 \text{ km s}^{-1}$ and the chosen cluster radius (1 Mpc or R_{200}). This term is summed over all observed epochs, N_{ep} . Our control times are shorter than the 1 year of MENeACS survey time because SNe II are intrinsically fainter than the SNe Ia which MENeACS was designed to find.

For a cluster radius of 1 Mpc, the result is an expected number of interloping supernovae $N_{exp} = 0.2^{+0.2}_{-0.1}$. The Poisson probability that we observed 0, 1, or 2 SNe within 1 Mpc is $\sim 0.81, 0.17,$ and 0.02 respectively. Similarly for a cluster radius of R_{200} , $N_{exp} = 0.7^{+0.5}_{-0.3}$, and the probabilities of observing 0, 1, 2, or 3 SNe are $\sim 0.50, 0.35, 0.12,$ and 0.03 . For every realization of our Monte Carlo we randomly draw a value of $N_{exp} = 0, 1, 2,$ or 3 SNe, weighted by its respective probability, and subtract it from the number observed in order to produce SN II rates statistically corrected for interloping SNe. Since our one red sequence SN II host has a redshift consistent with the cluster *and* lies on the photometric red sequence – and considering that the number density of potential red sequence interlopers is relatively small – we consider it very unlikely to be an interloper, and we do not apply the interloper correction to the red sequence SNR_{II} .

4.3. MENeACS SN II Rates and Uncertainties

The MENeACS SN II cluster rates are presented in Table 4 in the conventional units of SNUB and SNUM, where $SNUB \equiv SNe(100 \text{ yr } 10^{10} L_{B,\odot})^{-1}$ and $SNUM \equiv SNe(100 \text{ yr } 10^{10} M_{\odot})^{-1}$. We present the rate in three cluster galaxy subsets: “All”, the total stellar mass including the intracluster stars; “RS”, red sequence galaxies only; and “Off RS”, galaxies lying off their cluster’s red sequence. We show our results with the SN II luminosity functions from both Li11a and C93a, and within cluster radii of 1 Mpc and R_{200} .

The statistical uncertainties include the Poisson error on the number of SNe II observed, the interloper contamination, the uncertainty on cluster luminosity, and the uncertainty in our detection efficiencies. Statistical errors are dominated by the Poisson uncertainties and interloper contamination (with relative contributions of $\sim 2/3$ and $\sim 1/3$, respectively), with very small uncertainties ($1\sim 5\%$) from our detection efficiency and cluster mass/luminosity uncertainty. The systematic uncertainties include a small contribution from the inclination correction factor (5%; Appendix A), an offset of $\sim 10\%$ in cluster luminosity which was derived from a comparison of MENeACS photometry to SDSS, and the uncertainty in R_{200} for rates within R_{200} (the latter two are discussed in detail in S12). The relative contributions to the systematic uncertainty from these two components is $\sim 30\%$ and 70% respectively.

4.4. Caveats

Here we make several important notes regarding the MENeACS SN II rate in clusters. First, ZwCl0628_7_08_0 was both $m_g > 22.5$ magnitudes and $g-r > 0.8$ at all detections, and therefore did not officially meet our follow-up requirements. Occasionally we followed-up targets outside our formal bounds, but despite its spectroscopic confirmation we cannot include ZwCl0628_7_08_0 in the

rates.

Second, our control time goes to zero for SN II fainter than $M_B \sim -14.6$ magnitudes, yielding an unphysical infinite rate. We exclude these realizations when calculating the median rate and its uncertainty, which is effectively the same as truncating the SN II LF at $M \sim -14.6$ magnitudes. This approach is valid because it is inappropriate to calculate the rates of objects to which a survey is insensitive. The result is that our rates are for the “normal” population of SNe II with $M_B \leq -14.6$ magnitudes, and do not include the faint sub-population found by Li11a. If we include the realizations of infinite rates in the median (e.g. for “All” galaxy types and R_{200}), the rate becomes 0.031 instead of 0.026 SNUM with the Li11a LF – a difference of $\lesssim 0.07\sigma$. For the C93a LF, the difference is also negligible. In Appendix B we discuss a rate calculation method which integrates over the SN II LF to avoid the instances of zero control times, and explain how it is not appropriate for MENeACS.

Third, as discussed in § 2 our sparse light curve sampling and single epoch spectroscopy means we cannot identify SN II subtypes P, L, b, or n. It is likely that the subtype distribution in clusters is similar to that in field S0-Sbc hosts reported by Li11a, so it is possible that our sample contains all SN IIP. For this reason, we also run our Monte Carlo using SN II LFs for the plateau subtype only. Figure 6 shows that the SN IIP LFs are fainter, and that the L, b, and n subtypes populate the magnitude bins brighter than -17.5. This leads to higher rates for SN IIP: 0.032 instead of 0.026 SNUM with the Li11a LF, which is a difference of $\lesssim 0.08\sigma$.

4.5. Comparison to Published SN II Rates

The only previous measure of the cluster SNR_{II} is from M08, who compiled five visual and photographic $z < 0.02$ galaxy-targeted SN searches in which “the original galaxy sample was not selected in order to reproduce the cosmic average but rather to have a significant number of SN detections”. This means that massive galaxies were preferentially targeted and associated with galaxy clusters later, and that the surveyed cluster mass of M08 is incomplete. Furthermore, SNe discovered during the surveys used by M08 were not all spectroscopically classified. MENeACS, on the other hand, surveyed galaxy clusters between $0.05 < z < 0.15$ to R_{200} , including the stellar mass in faint galaxies and the intracluster population, and uses only spectroscopically confirmed SNe. Although the MENeACS survey strategy is better, our survey duration is shorter, our discovered number of SNe II is smaller, and the Poisson uncertainties are larger. In general the M08 rates in Table 1 and the MENeACS rates in Table 4, for the variety of cluster radii and galaxy types considered, are consistent at the $1-2\sigma$ level.

A comparison of the rate of core collapse supernovae (SNR_{CC} , which includes Types II and Ibc) between cluster and field galaxies with similar SFRs can potentially reveal an environmental dependence of the initial mass function (IMF). For example, consider two galaxies with the same total star formation rate: if one has a higher SNR_{CC} , then it is forming a larger fraction of $\geq 8 M_{\odot}$ stars. We did not discover any SN Ibc. The Ibc:II ratio is typically 1:2 to 1:4 in cluster and field environments, respectively (M08; Li et al. 2011b). Based on this, we only expect 1.7–3.5 SNe Ibc, and the probability of ob-

serving zero is 3–18%. Thus, we are insensitive to any environmental dependence of the IMF at masses $\geq 20 M_{\odot}$. A comparison of the MENeCS SNR_{II} in cluster “RS” and “Off-RS” galaxies to the published rates in field E/S0 and S0a/b galaxies in Table 1 finds a general $1-2\sigma$ agreement. We conclude that SN II cluster rates require a more precise measurement in order to firmly identify any difference in the cluster IMF.

5. CLUSTER STAR FORMATION RATES

We begin our discussion with the first-ever derivation of cluster SFR from SNe II, which we compare with other measurements of cluster SFR, in § 5.1. In § 5.2 we discuss the MENeCS limits on intracluster star formation. In § 5.3 we discuss the implications of cluster SF for SNe Ia, including whether short-delay SNe Ia contaminate the late-time DTD when measured via the cluster SNIa rate; the possibility that all SNe Ia have short delays; and the potential source of the SNR_{Ia} enhancement in cluster ellipticals observed by M08.

5.1. Derivation of Cluster SFR from SN II Rates

Botticella et al. (2012) present a derivation of the relation between the CCSN rate and SFR , which we adapt to SN II:

$$R_{II} = K_{II} \times SFR. \quad (4)$$

In the above expression, R_{II} is the rate of SN II with units of SN yr^{-1} (whereas SNR_{II} is in units of $\text{SNUM} = \text{SN} (10^2 \text{yr})^{-1} (10^{10} M_{\odot})^{-1}$). The value of R_{II} is calculated in a similar manner as SNR_{II} , and presented in Table 5. The SFR is in units of $M_{\odot} \text{yr}^{-1}$, and K_{II} is the number fraction of all stars formed which explode as SN II ($\text{SN } M_{\odot}^{-1}$):

$$K_{II} = \frac{\int_{m_{l,II}}^{m_{u,II}} \phi(m) dm}{\int_{m_l}^{m_u} m \phi(m) dm}. \quad (5)$$

The integration limits $m_{l,II}$ and $m_{u,II}$ correspond to the minimum and maximum initial masses of stars which become SNe II. The lower limit is generally agreed to be $\sim 8 M_{\odot}$, and evidence is converging towards an upper limit of $\lesssim 20 M_{\odot}$ (e.g. Smartt et al. 2009; Dessart et al. 2010). For $\phi(m)$, the initial mass function (IMF), we use the Salpeter expression where $\phi(m) \propto m^{\gamma}$, and $\gamma = -2.35$ (Salpeter 1955). The limits m_l and m_u are the mass range of the IMF, for which we use 0.1 and $100 M_{\odot}$. Under these assumptions, $K_{II} = 0.0054$. By extending m_l and m_u to 0.05 and 200, testing a slightly lower exponent of $\gamma = -2.3$ (Kroupa 2001), and considering a lower $m_{u,II} = 17 M_{\odot}$, we estimate an uncertainty on K_{II} of ± 0.001 . We account for this with a $\sim 18\%$ systematic on the cluster SFR . We also calculate the specific star formation rate as $sSFR = SNR_{II}/K_{II}$, and list them in Table 5.

We now compare with a selection of previous cluster SFR measurements from IR and UV imaging, and optical spectroscopy. Chung et al. (2011) used WISE images of 72 low redshift ($z < 0.1$) galaxy clusters at wavelengths 3.4, 4.6, 12, and $22 \mu\text{m}$. They found that for $0.5 < R < 1 R_{200}$, clusters have a mean $sSFR \sim 2 M_{\odot} \text{yr}^{-1} (10^{12} M_{\odot})^{-1}$ (see their Figure 3). Our measurement for “All” galaxy types in clusters, $sSFR =$

$5.1_{-3.1}^{+15.8} \pm 0.9 M_{\odot} \text{yr}^{-1} (10^{12} M_{\odot})^{-1}$, is in agreement with this. Yi et al. (2005) used GALEX UV images to look for evidence of recent SF in SDSS field early-type galaxies. They found that 1–2% of the stellar mass in $\sim 15\%$ of bright ($M_R < -22$ magnitudes) early-types formed within the last ~ 1 Gyr. If this is true for clusters, we would expect $SFR = 2-4 M_{\odot} \text{yr}^{-1}$ in bright red sequence galaxies. If true for fainter red sequence members also, the expected total SFR raises to $10-20 M_{\odot} \text{yr}^{-1}$, which is ~ 5 times higher than (but within 2σ of) our red sequence SFR, $2.1_{-0.9}^{+2.0} \pm 0.4 M_{\odot} \text{yr}^{-1} (10^{12} M_{\odot})^{-1}$. Based on the $H\alpha$ luminosity from SDSS optical spectra, Finn et al. (2008) determined that $sSFR \sim 9 M_{\odot} \text{yr}^{-1} (10^{12} M_{\odot})^{-1}$ for star-forming galaxies in low redshift clusters. This is in 1σ agreement with our “Off-RS” $sSFR = 16.6_{-9.6}^{+39.5} \pm 3.0 M_{\odot} \text{yr}^{-1} (10^{12} M_{\odot})^{-1}$.

Finally, we note that our low $sSFR$ in red sequence galaxies implies that only $\sim 0.01\%$ of the mass in the red sequence at $z \sim 0.1$ is comprised of stars formed in the past 50 Myr. This extremely low percentage is consistent with the lack of detection in UV and IR of the red sequence host of Abell399.11.19.0 presented in § 3.

5.2. Intracluster Star Formation

Direct evidence of intracluster star formation has been presented by Sun et al. (2010), who detected a 40 kpc long X-ray tail extending from a galaxy in a nearby rich cluster. With optical spectra they identified 35 H II regions along this tail, the furthest of which are 20 kpc away from the galaxy (far enough to be defined as intracluster). Also, simulations of galaxy clusters investigating the size and origin of the IC stellar population suggest that $\sim 30\%$ of the IC stars form at significant distances from a galaxy dark matter halo (Puchwein et al. 2010). In such simulations most of the IC stars form at $z > 1$, with just a small tail of $\sim 1.5\%$ of the final IC stellar mass forming during the last ~ 1.8 Gyr (since $z = 0.15$). For the average IC stellar mass of our clusters, assuming an IC mass fraction of 16–45% (Gonzales et al. 2005; S11), this implies an IC SFR of $5-13 M_{\odot} \text{yr}^{-1}$, and $R_{II} = 0.019-0.049 \text{ SN II yr}^{-1}$. This converts into an expectation of 0.3–0.8 IC SNe II in the MENeCS sample, which is consistent with our observation of zero. Interestingly, if the Puchwein et al. (2010) simulations are correct, the first detection of an IC SN II would be likely in a survey just twice as large as MENeCS.

Although we know our upper limit on the IC SFR will not be very restrictive, it is the first derived from the non-detection of IC SNe II. This is only possible in a complete, well characterized survey like MENeCS. To calculate an upper limit for the rate of IC SNe II within R_{200} , we use Poisson statistics for a detection of zero (Gehrels 1986), and allow fractional values of IC N_{II} in the Monte Carlo rate calculation represented by Equation 1 (with $C_{inc} = 1.0$). The resulting 1σ upper limit is $R_{II} < 0.15 \text{ SN yr}^{-1}$, which converts to an upper limit of IC $SFR < 28 M_{\odot} \text{yr}^{-1}$.

5.3. Implications For Cluster SNe Ia

In § 1 we described how deducing the late-time SNIa DTD from the cluster SNR_{Ia} as a function of redshift must assume that cluster stars all formed in a burst at high redshift, and that all cluster SNe Ia have experi-

enced a long, > 2 Gyr, delay time. In this section we explore the impact of cluster star formation on this assumption, and its implications for the SN Ia DTD. First, we discuss our results with respect to the possibility of prompt-only SN Ia DTD. Next, we estimate the contamination of “prompt” SNe Ia to the cluster sample at low redshift. Finally, we comment on the implications of our cluster SNR_{II} and SFR regarding the source of the enhanced SNR_{Ia} in cluster ellipticals presented by M08.

5.3.1. A DTD of Short Delays Only?

Maoz et al. (2010) find that the cluster SNR_{Ia} as a function of redshift is best and most simply fit by a brief burst of star formation at $z \sim 3$ combined with a SN Ia DTD that peaks at short delays of < 2 Gyr and decreases as a power law with a slope of -1 to long delays of ~ 11 Gyr. This DTD is consistent with theoretical predictions of the double degenerate scenario. They also consider a DTD of short delays only, congruent with predictions for the single-degenerate model. They find it can only reproduce the observed cluster $SNR_{Ia}(z)$ from $0 < z < 1.2$ if they include ongoing cluster star formation within a radius of 1 Mpc.

Maoz et al. (2010) reject the prompt-only DTD hypothesis in part because previous surveys found SNe Ia mainly within 1 Mpc and always in elliptical, red sequence galaxies showing no signs of star formation, and in part due to other work showing cluster star formation was predominantly outside of 1 Mpc. With MENeACS, we have shown that SNe Ia do occur outside of 1 Mpc, and in blue cluster galaxies (Figure 2, and S12). We have also shown that SNe II, and therefore star formation, occurs inside of 1 Mpc and in red sequence galaxies.

Qualitatively, this suggests it would be premature to rule out a DTD of short delays only, and the single-degenerate model as the sole scenario, based on observed SNe Ia cluster rates. Quantitatively, Maoz et al. (2010) find that a SN Ia DTD of short delays only requires a rate of ongoing star formation $SFR \sim 175 M_{\odot} \text{ yr}^{-1}$ in the central regions of galaxy clusters. This is ~ 3 times higher than our cluster SFR inferred from SNe II, but our uncertainties on cluster SFR are large, and $175 M_{\odot} \text{ yr}^{-1}$ is actually just within the 1σ upper limit. Ultimately, although our cluster SFR rate is low, we cannot rule out a DTD of short delays only.

5.3.2. Fraction of “Prompt” Cluster SNe Ia

The SN Ia rate per unit mass, SNR_{Ia} , is a convolution of star formation history of the surveyed galaxy sample and the SN Ia DTD. As an oversimplified parametrization, it can be expressed as the sum of “delayed” and “prompt” components represented by constants A and B , where $SNR_{Ia} = A + B \times sSFR$ (Mannucci et al. 2005; Scannapieco & Bildsten 2005; Sullivan et al. 2006). Based on this, the fraction of SNe Ia expected to be associated with the prompt component is: $f_{prompt} = (B \times sSFR) / SNR_{Ia}$. We use the B value from Sullivan et al. (2006), $3.9 \pm 0.7 \times 10^{-4} \text{ SN yr}^{-1} (M_{\odot} \text{ yr}^{-1})^{-1}$. For MENeACS red sequence cluster galaxies, our derived $sSFR$ is in Table 5 and $SNR_{Ia} = 0.041^{+0.015+0.005}_{-0.015-0.010}$ SNum (S12). This reveals $f_{prompt} = 0.02^{+0.05}_{-0.02}$ in cluster red sequence galaxies; similarly, $f_{prompt} = 0.05^{+0.19}_{-0.05}$ for “All” cluster galaxies.

While this minimal $\sim 2\%$ contamination indicates that all of the MENeACS SNe Ia likely experienced a long delay time, we cannot rule out that up to 7% of SNe Ia in red sequence hosts exploded with short delay times (the 1σ confidence level). If so, then the “RS” SNR_{Ia} for the delayed SNe Ia only would be ~ 0.038 instead of 0.041 SNum. This is a difference of 0.003 SNum or, expressed in terms of the uncertainty on SNR_{Ia} , $\sim 0.2\sigma$. Ultimately, we find the potential maximum contamination from “prompt” SNe Ia is less than our statistical uncertainty on the cluster SN Ia rate. However, this may not be the case for higher redshift SN Ia cluster surveys.

5.3.3. The Enhanced SNR_{Ia} in Cluster Ellipticals

The rate of SNe Ia in cluster early-type galaxies was found to be a factor of three higher than the rate in field early-types by M08: $SNR_{Ia} = 0.066$ SNum compared to 0.019 SNum, respectively. They report that if this excess is from the “prompt” component, they would only expect ~ 2 SNe II – consistent with their detection of no SNe II in E/S0 hosts. In S12, we report the cluster red sequence $SNR_{Ia} = 0.041^{+0.015+0.005}_{-0.015-0.010}$ SNum, which is an excess of 0.022 SNum over the rate in field early-types from M08 (but given the uncertainties still consistent). Assuming this is entirely from the prompt component, and using the B value from Sullivan et al. (2006), we find an implied $sSFR = 56^{+38}_{-45} M_{\odot} \text{ yr}^{-1} (10^{12} M_{\odot})^{-1}$ in cluster red sequence galaxies. This is a factor of ~ 28 times greater than our observed SFR in Table 5. If we instead consider our “All” galaxy sample the implied $sSFR = 56^{+40}_{-34} M_{\odot} \text{ yr}^{-1} (10^{12} M_{\odot})^{-1}$ is a factor of ~ 11 times greater than the observed SFR in clusters. Given that the relation between SFR and SNR_{II} is direct (Equation 4), then we should have observed an order of magnitude more SNe II in MENeACS. Our data suggests that either the SN Ia rate enhancement in cluster ellipticals does not exist, or it is not due to recent star formation.

6. CONCLUSION

In this paper we present the 7 SNe II discovered in $0.05 < z < 0.15$ rich galaxy clusters by MENeACS. Our sample also includes one SN II in a red sequence galaxy which shows no clear evidence of recent star formation in its multi-wavelength properties. This illustrates the danger of using host morphology to classify SNe in lieu of expensive spectroscopy time. The simplest explanation is that undetectable levels of star formation exist in the elliptical host. If that is not the case, it leaves open the possibility of a rare other channel to SNe II with a long delay time.

With the MENeACS sample we make the first measurement of SNR_{II} from a survey which is both cluster-targeted and complete to R_{200} . We also make the first derivation of cluster SFR from SNR_{II} , and find that it agrees with SFR measurements for cluster galaxies and field ellipticals from IR and UV photometry, and $H\alpha$ line emission. We show how these low levels of cluster star formation imply that a small fraction of cluster SNe Ia may have experienced a short delay time. However, we find their influence on the cluster SNR_{Ia} is within statistical uncertainties, and does not undermine the use of low redshift cluster $SNR_{Ia}(z)$ to derive the delay time distribution for SNe Ia.

We gratefully acknowledge the CFHT Queued Service Observations team, without whom MENeCS would not have been possible. We thank Nelson Caldwell for managing the MMT/Hectospec queue, and also thank Stephenson Yang for his dedication to essential computer and network maintenance. CJP acknowledges support from the National Engineering and Science Research Council of Canada. HH acknowledges support from a Marie Curie International Reintegration Grant and the NWO Vidi grant. This work is based in part on data products produced at the Canadian Astronomy Data Centre as part of the Canada-France-Hawaii Telescope Legacy Survey, a collaborative project of NRC and CNRS. This work is based on observations obtained with MegaPrime/MegaCam, a joint project of CFHT and CEA/DAPINA, at the Canada-France-Hawaii Telescope (CFHT) which is operated by the National Research Council (NRC) of Canada, the Institut National des Sciences l'Universe of the Centre National de la Recherche Scientifique (CNRS) of France, and the University of Hawaii. Observations reported here were obtained at the MMT Observatory, a joint facility of the Smithsonian Institution and the University of Arizona. This research has made use of the VizieR catalogue access tool, CDS, Strasbourg, France. This research has made use of the NASA/IPAC Extragalactic Database (NED) which is operated by the Jet Propulsion Laboratory, California Institute of Technology, under contract with the National Aeronautics and Space Administration. This research has made use of the NASA/IPAC Infrared Science Archive, which is operated by the Jet Propulsion Laboratory, California Institute of Technology, under contract with the National Aeronautics and Space Administration. This publication makes use of data products from the Wide-field Infrared Survey Explorer, which is a joint project of the University of California, Los Angeles, and the Jet Propulsion Laboratory/California Institute of Technology, funded by the National Aeronautics and Space Administration.

Facilities: CFHT, MMTO, Gemini.

REFERENCES

- Adams, S. M. et al. 2012, in preparation
- Barbary, K. et al. 2012, *ApJ*, 745, 32
- Bazin, G. et al. 2009, *A&A*, 499, 653
- Bianchi, L., Herald, J., Efremova, B., Girardi, L., Zobot, A., Marigo, P., Conti, A., and Shiao, B. 2011, *Ap&SS*, tmp, 246B
- Bildfell, C. J. et al. 2012, *MNRAS*, submitted [arXiv:1202.6058]
- Blondin, S. & Tonry, J. L. 2007, *ApJ*, 666, 1024
- Botticella, M.T., Smartt, S.J., Kennicutt, Jr., R.C., Cappellaro, E., Sereno, M., and Lee, J.C. 2012, *A&A*, 537, 132
- Boulaide et al. 2003, in *Society of Photo-Optical Instrumentation Engineers (SPIE) Conference Series*, Vol. 4841, Society of Photo-Optical Instrumentation Engineers (SPIE) Conference Series, ed. M. Iye & A. F. M. Moorwood, 72–81
- Cappellaro, E., Turatto, M., Benetti, S., Tsvetkov, D. Yu., Bartunov, O. S. and Makarova, I. N. 1993a, *A&A*, 268, 472
- Cappellaro, E., Turatto, M., Benetti, S., Tsvetkov, D. Yu., Bartunov, O. S. and Makarova, I. N. 1993b, *A&A*, 273, 383
- Cappellaro, E., Turatto, M. and Evans, R. 1999, *A&A*, 351, 459
- Chary, R. & Elbaz, D. 2001, *ApJ*, 556, 562
- Chilingarian, I. V., Melchior, A.-L., and Zolotukhin, I. Y. 2010, *MNRAS*, 405, 1409.
- Chung, S. M., Eisenhardt, P. R., Gonzalez, A. H., Stanford, S. A., Brodwin, M., Stern, D., and Jarrett, T. 2011, *ApJ*, 743, 34
- D’Andrea, C. B. et al. 2010, *ApJ*, 708, 661
- Dessart, L., Livne, E., and Waldman, R. 2010, *MNRAS*, 408, 827
- Elias-Rosa, N., Van Dyk, S. D., Li, W., Silverman, J. M., Foley, R. J., Ganeshalingam, M., Mauerhan, J. C., Kankare, E., Jha, S., Filippenko, A. V., Beckman, J. E., Berger, E., Cuillandre, J.-C., and Smith, N. 2011, *ApJ*, 742, 6
- Eisenhardt, P. R. M. et al. 2008, *ApJApJ*, 684, 905
- Fabricant, D. et al. 2005, *PASP*, 117, 1411
- Filippenko, A. V. 1997, *ARA&A*, 35, 309
- Finn, R. A., Balogh, M. L., Zaritsky, D., Miller, C. J. & Nichol, R. C. 2008, *ApJ*, 679, 279
- Fioc, M. & Rocca-Volmerange, B. 1997, *A&A*, 326, 950
- Fritz, J. et al. 2011, *A&A*, 526, 45
- Gal-Yam, A., Leonard, D. C., Fox, D. B., Cenko, S. B., Soderberg, A. M., Moon, D.-S., Sand, D. J., Caltech Core Collapse Program, Li, W., Filippenko, A. V., Aldering, G. and Copin, Y. 2007, *ApJ*, 656, 372
- Gehrels, N. 1986, *ApJ*, 303, 336
- Graham, M. L. et al. 2010, *AJ*, 139, 594
- Gonzalez, A. H., Zabludoff, A. I., & Zaritsky, D. 2005, *ApJ*, 618, 195
- Hakobyan, A. A., Petrosian, A. R., McLean, B., Kunth, D., Allen, R. J., Turatto, M., & Barbon, R. 2008, *A&A*, 488, 523
- Hamuy, M. 2003, *ApJ*, 582, 905
- Heney, L.G., Lelevier, R., Levee, R.D. 1959, *ApJ*, 129, 2
- Hogg, D. W. 1999, [arXiv:9905116]
- Howell, D. A. et al. 2005, *ApJ*, 634, 1190
- Jester, S. et al. 2005, *AJ*, 130, 873
- Kaviraj, S. 2010, *MNRAS*, 408, 170
- Kewley, L. J., Groves, B., Kauffmann, G., and Heckman, T. 2006, *MNRAS*, 372, 961
- Kinney, A. L. et al. 1996, *ApJ*, 467, 38
- Krisciunas, K. et al. 2009, *ApJ*, 137, 34
- Kroupa, P. 2001, *MNRAS*, 322, 231
- Leaman, J., Li, W., Chornock, R., and Filippenko, A. V. 2011, *MNRAS*, 412, 1419
- Li, W., Wang, X., Van Dyk, S. D., Cuillandre, J., Foley, R. J., Filippenko, A. V. 2007a, *ApJ*, 661, 1013
- Li, Z., Han, Z. and Zhang, F. 2007b, *A&A*, 464, 853
- Li, W., Leaman, J., Chornock, R., Filippenko, A. V., Poznanski, D., Ganeshalingam, M., Wang, X., Modjaz, M., Jha, S., Foley, R. J., and Smith, N. 2011, *MNRAS*, 412, 1441
- Li, W., Chornock, R., Leaman, J., Filippenko, A. V., Poznanski, D., Wang, X., Ganeshalingam, M., and Mannucci, F. 2011, *MNRAS*, 412, 1473
- Maltby, D. T., Hoyos, C., Gray, M. E., Aragón-Salamanca, A. and Wolf, C. 2011, *MNRAS*, tmp.1649M
- Mannucci, F., Della Valle, M., Panagia, N., Cappellar, E., Cresci, G., Maiolino, R., Petrosian, A. and Turatto, M. 2005, *A&A*, 433, 807
- Mannucci, F., Maoz, D., Sharon, K., Botticella, M. T., Della Valle, M., Gal-Yam, A. and Panagia, N. 2008, *MNRAS*, 383, 1121
- Maoz, D. & Gal-Yam, A. 2004, *MNRAS*, 347, 951
- Maoz, D., Sharon, K. & Gal-Yam, A. 2010, *ApJ*, 722, 1879
- Maoz, D. & Mannucci, F. 2011, [arXiv:1111.4492]
- Maund, J. R., Fraser, M., Ergon, M., Pastorello, A., Smartt, S. J., Sollerman, J., Benetti, S., Botticella, M.-T., Bufano, F., Danziger, I. J., Kotak, R., Magill, L., Stephens, A. W. and Valenti, S. 2011, *ApJ*, 739, 37
- Million, E.T., Werner, N., Simionescu, A., Allen, S.W. 2011, *MNRAS*, 418, 2744
- Nugent, P., Kim, A. and Perlmutter S. 2002, *PASP*, 114, 803
- Oke, J. B. 1974, *ApJS*, 27, 21
- Olivares E., F. et al. 2010, *ApJ*, 715, 833
- Perlmutter, S. et al. 1997, *ApJ*, 483, 565
- Phillips, M. 1993, *ApJ*, 413, 105
- Poznanski, D., Gal-Yam, A., Maoz, D., Filippenko, A. V., Leonard, D. C. and Matheson, T. 2002, *PASP*, 114, 833
- Pritchett, C. J., Howell, D. A., & Sullivan, M. 2008, *ApJ*, 683, 25
- Puchwein, E., Springel, V., Sijacki, D., & Dolag, K. 2010, *MNRAS*, 406, 936
- Rudnick, G. et al. 2009, *ApJ*, 700, 1559
- Salpeter, E. E., 1955, *ApJ*, 121, 161
- Sand, D. J. et al. 2011, *ApJ*, 729, 142
- Sand, D. J. et al. 2012, *ApJ*, 746, 163
- Sanders, J.S. & Fabian, A.C. 2006, *MNRAS*, 371, 1483
- Sato, K., Tokoi, K., Matsushita, K., Ishisaki, Y., Yamasaki, N. Y., Ishida, M. and Ohashi, T. 2007, *ApJ*, 667, 41
- Scannapieco, E. & Bildsten, L. 2005, *ApJ*, 629, 85
- Schawinski, K. 2009, *MNRAS*, 397, 717
- Schmidt, G. D., Weymann, R. J. & Foltz, C. B. 1989, *PASP*, 101, 713
- Sharon, K., Gal-Yam, A., Maoz, D., Filippenko, A. V. and Guhathakurta, P. 2007, *ApJ*, 660, 1165
- Smartt, S. J., Eldridge, J. J., Crockett, R. M., & Maund, J. R. 2009, *MNRAS*, 395, 1409
- Stanford, S. A., Eisenhardt, P. R., and Dickinson, M. 1998, *ApJ*, 492, 461
- Suh, H., Yoon, S., Jeong, H. and Yi, S. K. 2011, *ApJ*, 730, 110
- Sullivan, M. et al. 2006, *ApJ*, 648, 868
- Sun, M., Donahue, M. & Voit, G. M. 2010, *ApJ*, 671, 190
- Wright, E. L. et al. *AJ*, 140, 1868
- Yi, S. K. et al. 2005, *ApJ*, 619, 111

TABLE 1
 PUBLISHED SN II RATES

Environment	Galaxy Types	Rate SNU ^B ^a	Rate SNU ^M ^b
Mannucci et al. (2008)			
Cluster	Total	$0.23^{+0.09}_{-0.07}$	$0.072^{+0.028}_{-0.021}$
Cluster	E/S0	< 0.071	< 0.017
Cluster	S0a/b	$0.17^{+0.19}_{-0.10}$	$0.061^{+0.068}_{-0.036}$
Cluster	Sbc/d	$0.87^{+0.41}_{-0.29}$	$0.610^{+0.290}_{-0.206}$
Field	Total	$0.44^{+0.08}_{-0.07}$	$0.174^{+0.032}_{-0.027}$
Field	E/S0	< 0.08	< 0.020
Field	S0a/b	$0.36^{+0.14}_{-0.10}$	$0.130^{+0.049}_{-0.037}$
Field	Sbc/d	$0.83^{+0.21}_{-0.17}$	$0.652^{+0.164}_{-0.134}$
Li et al. (2011b)			
Field	E	< 0.014	< 0.003
Field	S0	$0.200^{+0.015}_{-0.09}$ (0.006)	$0.005^{+0.004}_{-0.002}$ (0.001)
Field	Sab	$0.266^{+0.047}_{-0.041}$ (0.098)	$0.098^{+0.018}_{-0.015}$ (0.035)
Field	Sb	$0.282^{+0.043}_{-0.037}$ (0.106)	$0.144^{+0.023}_{-0.020}$ (0.055)
Field	Sbc	$0.466^{+0.058}_{-0.052}$ (0.134)	$0.355^{+0.042}_{-0.038}$ (0.098)
Field	Sc	$0.649^{+0.088}_{-0.078}$ ($+0.364$ -0.137)	$0.547^{+0.075}_{-0.066}$ ($+0.245$ -0.112)
Field	Scd	$0.795^{+0.097}_{-0.086}$ ($+0.386$ -0.135)	$0.767^{+0.116}_{-0.102}$ ($+0.342$ -0.154)

^a SNU^B \equiv SNe(100 yr $10^{10} L_{B,\odot}$)⁻¹
^b SNU^M \equiv SNe(100 yr $10^{10} M_{\odot}$)⁻¹

 TABLE 2
 MENEACS TYPE II CLUSTER SUPERNOVAE SPECTROSCOPY SUMMARY

MENEACS ID	UT Date	Telescope/ Instrument	Cluster z	Galaxy z	SNID z	SNID Template Type, Name	SNID Phase (σ) days	Exposure Time seconds
Abell119_5_24_0	2009-09-19.29	MMT/BCS	0.044	0.0480	0.050 (0.005)	IIP, SN92H	39.5 (88.0)	1200.0
Abell1795_8_08_1	2009-06-15.27	MMT/BCS	0.063	0.0626	0.0636 (0.0054)	IIP, SN04et	21.4 (55.8)	900.0
Abell399_11_19_0	2009-12-19.27	MMT/Hecto	0.072	0.072	0.0676 (0.0025)	IIP, SN04et	60.1 (19.2)	3600.0
Abell1651_7_05_3	2009-06-15.20	MMT/BCS	0.085	...	0.0739 (0.0050)	IIP, SN04et	26.9 (20.9)	900.0
ZwCl0628_7_08_0	2009-09-19.49	MMT/BCS	0.081	...	0.0759 (0.0050)	IIP, SN04et	48.2 (37.4)	900.0
Abell2443_5_19_0	2009-06-15.42	MMT/BCS	0.108	0.1106	0.1053 (0.0056)	IIP, SN99em	24.0 (15.5)	2400.0
Abell990_6_13_0	2009-03-16.11	MMT/Hecto	0.144	0.1425	0.1422 (0.0039)	IIP, SN04et	14.3 (10.8)	3600.0

 TABLE 3
 MENEACS TYPE II CLUSTER SUPERNOVAE HOST PROPERTIES

MENEACS ID	α J2000.0	δ J2000.0	r mag	$g-r$ mag	$\Delta(g-r)_{RS}$ mag	R_{clus} kpc	R_{clus} R_{200}
Abell119_5_24_0	00:55:39.69	-00:52:35.9	16.53 ± 0.02	0.40 ± 0.04	-0.41	1280	0.78
Abell1795_8_08_1	13:48:38.56	+26:22:18.5	20.23 ± 0.02	0.31 ± 0.04	-0.37	980	0.46
Abell399_11_19_0	02:57:16.58	+13:08:34.3	16.28 ± 0.02	0.85 ± 0.04	-0.02	920	0.49
Abell1651_7_05_3	12:57:23.39	-04:33:52.7	22.26 ± 0.06	0.22 ± 0.10	-0.45	3530	1.73
ZwCl0628_7_08_0	06:31:03.31	+24:49:17.8	16.11 ± 0.02	0.79 ± 0.05	-0.15	1170	0.73
Abell2443_5_19_0	22:25:07.59	+17:35:00.9	17.35 ± 0.02	0.56 ± 0.04	-0.43	2350	1.47
Abell990_6_13_0	10:23:18.58	+49:05:17.8	20.97 ± 0.03	0.32 ± 0.05	-0.63	730	0.39

TABLE 4
MENEACS CLUSTER SN II RATES

Galaxy Types	Radius	N_{SN}	SNuB ^a	SN II Rates	SNuM ^b
With the SN II LF of Li et al. (2010).					
All	1 Mpc	3	$0.137^{+0.318}_{-0.092}$ (stat) $^{+0.024}_{-0.018}$ (sys)	$0.032^{+0.074}_{-0.020}$ (stat) $^{+0.006}_{-0.004}$ (sys)	
All	R ₂₀₀	4	$0.093^{+0.235}_{-0.067}$ (stat) $^{+0.063}_{-0.012}$ (sys)	$0.026^{+0.075}_{-0.018}$ (stat) $^{+0.010}_{-0.003}$ (sys)	
RS	1 Mpc	1	$0.044^{+0.132}_{-0.044}$ (stat) $^{+0.005}_{-0.004}$ (sys)	$0.011^{+0.035}_{-0.011}$ (stat) $^{+0.001}_{-0.001}$ (sys)	
RS	R ₂₀₀	1	$0.028^{+0.061}_{-0.028}$ (stat) $^{+0.061}_{-0.003}$ (sys)	$0.007^{+0.014}_{-0.007}$ (stat) $^{+0.009}_{-0.001}$ (sys)	
Off RS	1 Mpc	2	$0.346^{+0.968}_{-0.346}$ (stat) $^{+0.061}_{-0.045}$ (sys)	$0.129^{+0.443}_{-0.129}$ (stat) $^{+0.023}_{-0.017}$ (sys)	
Off RS	R ₂₀₀	3	$0.220^{+0.499}_{-0.220}$ (stat) $^{+0.362}_{-0.029}$ (sys)	$0.080^{+0.179}_{-0.064}$ (stat) $^{+0.079}_{-0.013}$ (sys)	
With the SN II LF of Cappellaro et al. (1993a).					
All	1 Mpc	3	$0.112^{+0.931}_{-0.073}$ (stat) $^{+0.020}_{-0.015}$ (sys)	$0.035^{+0.231}_{-0.025}$ (stat) $^{+0.006}_{-0.005}$ (sys)	
All	R ₂₀₀	4	$0.088^{+0.665}_{-0.063}$ (stat) $^{+0.055}_{-0.011}$ (sys)	$0.026^{+0.168}_{-0.019}$ (stat) $^{+0.010}_{-0.004}$ (sys)	
RS	1 Mpc	1	$0.035^{+0.165}_{-0.035}$ (stat) $^{+0.004}_{-0.003}$ (sys)	$0.008^{+0.041}_{-0.008}$ (stat) $^{+0.001}_{-0.001}$ (sys)	
RS	R ₂₀₀	1	$0.023^{+0.154}_{-0.023}$ (stat) $^{+0.049}_{-0.002}$ (sys)	$0.005^{+0.047}_{-0.005}$ (stat) $^{+0.012}_{-0.000}$ (sys)	
Off RS	1 Mpc	2	$0.305^{+2.102}_{-0.305}$ (stat) $^{+0.054}_{-0.040}$ (sys)	$0.106^{+0.937}_{-0.106}$ (stat) $^{+0.019}_{-0.014}$ (sys)	
Off RS	R ₂₀₀	3	$0.194^{+0.994}_{-0.194}$ (stat) $^{+0.274}_{-0.028}$ (sys)	$0.067^{+0.518}_{-0.067}$ (stat) $^{+0.071}_{-0.010}$ (sys)	

^a SNuB \equiv SNe(100 yr $10^{10} L_{B,\odot}$)⁻¹

^b SNuM \equiv SNe(100 yr $10^{10} M_{\odot}$)⁻¹

TABLE 5
MENEACS CLUSTER STAR FORMATION RATES

Galaxy Types	N_{SN}	R _{II} SN yr ⁻¹	SFR M _⊙ yr ⁻¹	sSFR M _⊙ yr ⁻¹ ($10^{12}M_{\odot}$) ⁻¹
All	4	$0.308^{+0.912}_{-0.184}$	$56.6^{+167.3}_{-33.7}$ (stat) ± 10.2 (sys)	$5.1^{+15.8}_{-3.1}$ (stat) ± 0.9 (sys)
RS	1	$0.072^{+0.155}_{-0.032}$	$13.3^{+28.4}_{-5.8}$ (stat) ± 2.4 (sys)	$2.0^{+4.2}_{-0.9}$ (stat) ± 0.4 (sys)
Off RS	3	$0.225^{+0.466}_{-0.131}$	$41.3^{+85.6}_{-24.1}$ (stat) ± 7.4 (sys)	$16.6^{+39.5}_{-9.6}$ (stat) ± 3.0 (sys)

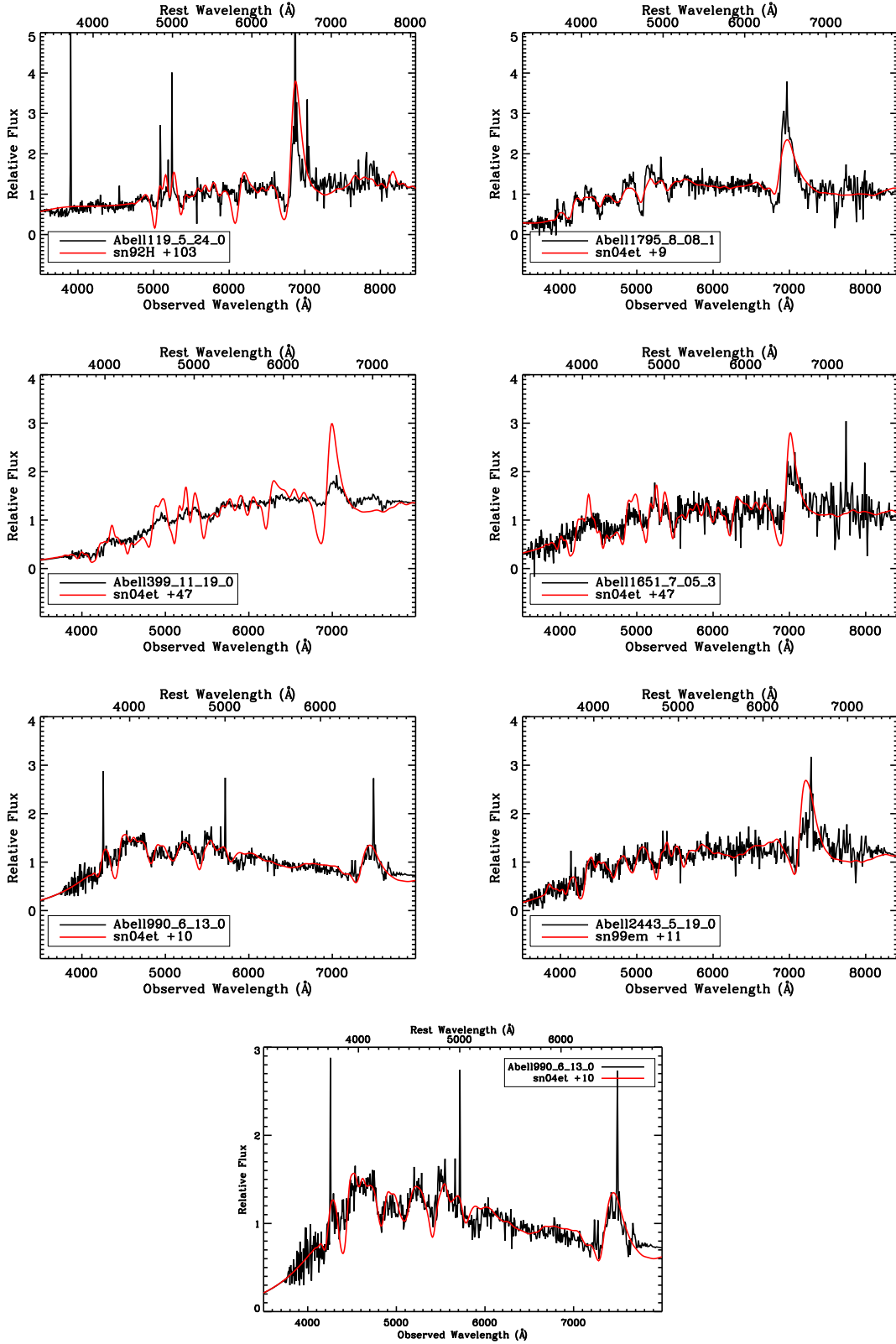


FIG. 1.— Spectra for our cluster SNeII in black, with the best fitting SN II template spectrum from SNID in red (see Table 2).

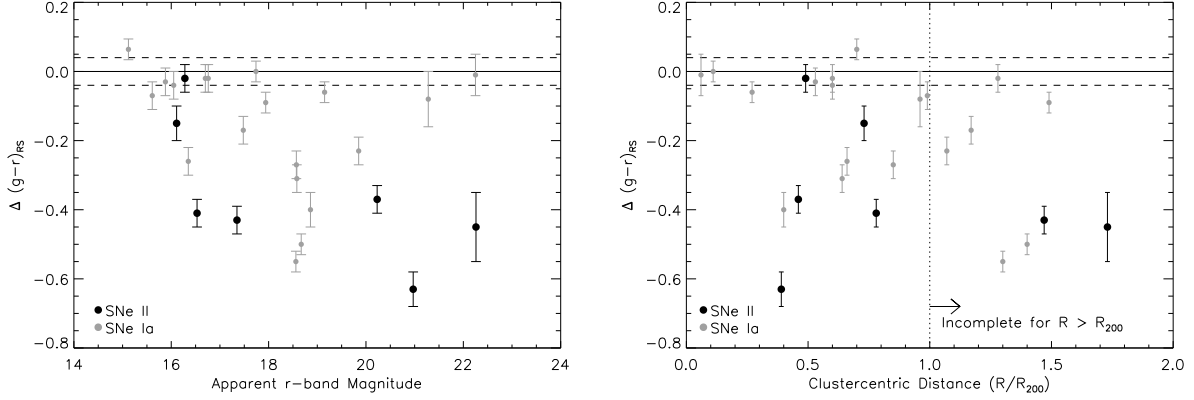


FIG. 2.— The offset of each SN II (black) and SN Ia (gray) host galaxy from its cluster’s red sequence, $\Delta(g-r)_{RS}$, versus the host galaxy r -band apparent magnitude (left) and the clustercentric offset in units of R_{200} (right). Dashed lines represent the median scatter in the red sequence over the whole MENeACS sample.

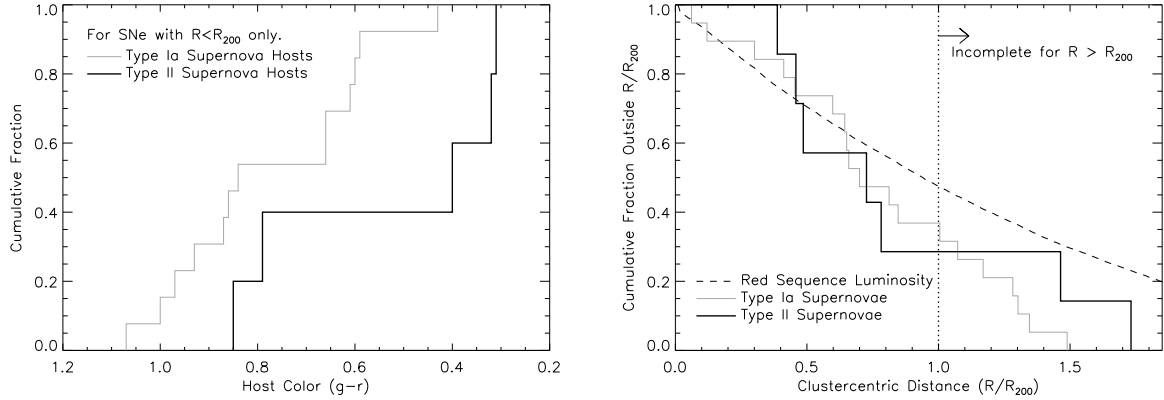


FIG. 3.— Left: The normalized cumulative distributions of SN Ia (gray) and SN II (black) host $g-r$ colors, for SNe within R_{200} . A two-sided KS test finds there a $< 10\%$ probability that these are drawn from the same underlying distribution. Right: normalized, cumulative g -band luminosity in red sequence galaxies (dashed), and the cumulative number fractions of SNe Ia (gray) and SNe II (black). Within R_{200} , the distribution of projected clustercentric offsets for SNe Ia appears to “follow the light” in the red sequence better than SNe II, as expected.

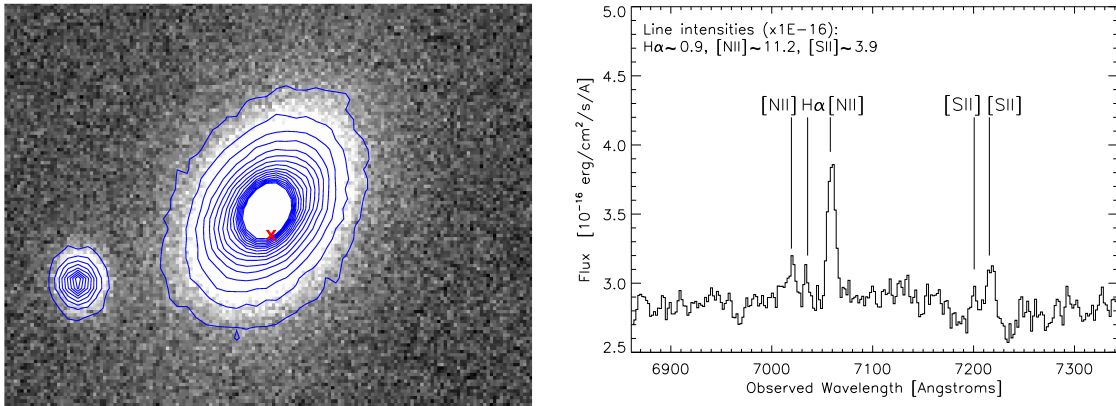


FIG. 4.— Left: The host of SN II Abell399_11_19_0, with the SN marked as a red cross, and smoothed isophotal contours to highlight this galaxy’s elliptical morphology. Right: A partial spectrum of the red sequence host galaxy of SN II Abell399_11_19_0, showing the relevant emission lines. Line intensities are estimated by integrating the flux over the line width.

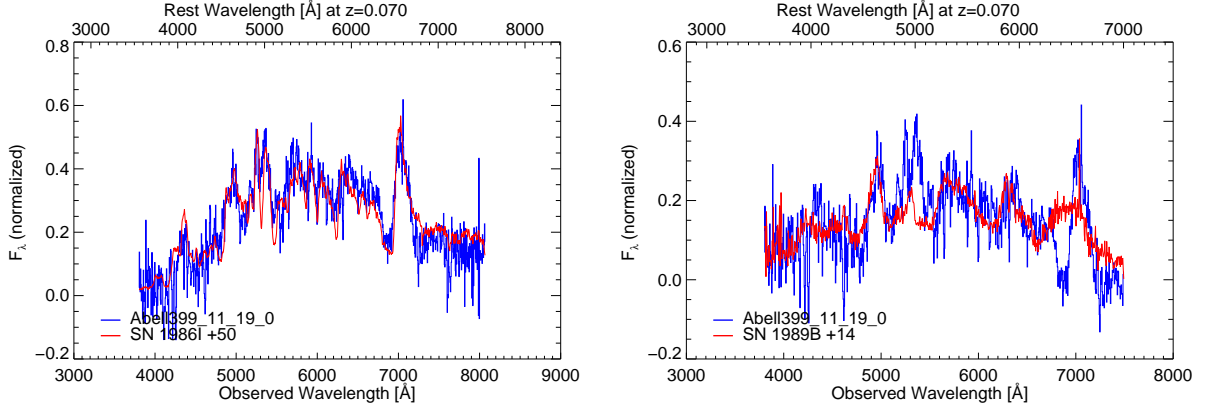


FIG. 5.— The best fitting template from Superfit (red) to the observed spectrum of Abell399_11_19_0 (blue, with best fitting host spectra subtracted), when considering only SN II (left) and only SN Ia (right) with the spectral template matching code Superfit (Howell et al. 2005). The best fit SN II template is a much better match than the best SN Ia template, in particular to the P-Cygni profile at $\sim 7000 \text{ \AA}$.

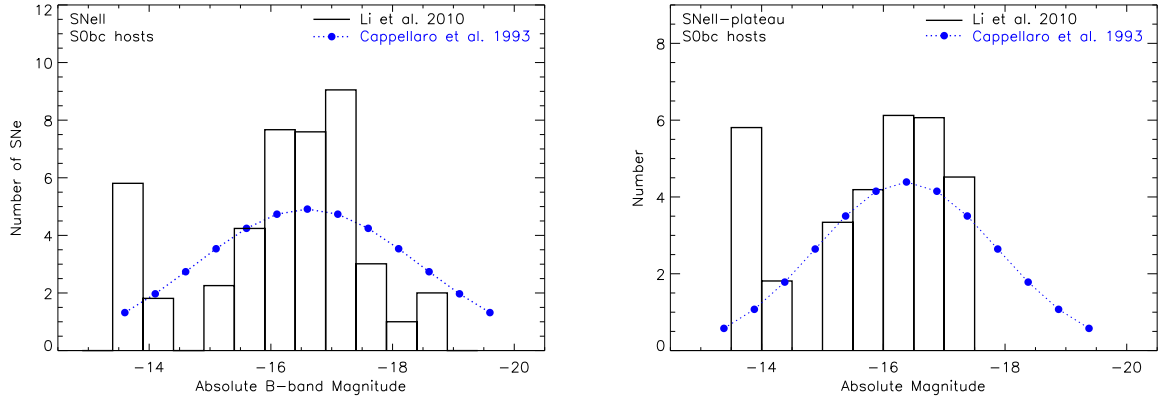


FIG. 6.— SN II luminosity functions. Black, the volume-limited SN II luminosity function observed by Li et al. (2010), for host galaxies of type S0-Sbc. Blue, the SN II luminosity function used by Cappellaro et al. (1993a), normalized to the same total number as the Li et al. (2010).

A. DERIVATION OF THE INCLINATION CORRECTION

A lower SNR_{II} has been observed in high inclination spiral galaxies relative to low inclination spirals (e.g. Cappellaro et al. 1993b; Cappellaro et al. 1999). This difference is attributed to dust obscuring SNe when our line of site goes through the disk. It was suggested by Cappellaro et al. (1993b) that this only affects photographic surveys. However, Li et al. (2011b) is a CCD survey and they report a strong trend between SNR_{II} and inclination for late-type spirals, but a very mild trend for early-type spirals.

Although the SN II LF of Lilla was not corrected for host extinction, using it does not mean we have included an inclination correction factor. For galaxy targeted SN surveys the inclination of each spiral galaxy is inferred from its shape, and the inclination correction derived from the observed rates. However, without redshifts for all galaxies in the CFHT MegaCam field of view, we cannot identify which spirals belong to the cluster and our inclination correction must be statistically estimated.

To derive our inclination correction factor, we first describe the simple case of having two samples of galaxies, “regular” and “inclined”. The fraction of SN II host galaxies which are “regular” is $f_{H(r)}$, the fraction which are “inclined” is $f_{H(i)}$, and the fraction of all occurring SNe II that *are* detected is $f_{SN_d(r)}$ and $f_{SN_d(i)}$. The inclination-corrected number of SNe II, $N_{II,c}$, given the total number observed, N_{II} , is $N_{II,c} = C_{inc}N_{II}$ where the inclination correction factor C_{inc} is:

$$C_{inc} = f_{H(r)} \frac{1}{f_{SN_d(r)}} + f_{H(i)} \frac{1}{f_{SN_d(i)}}. \quad (6)$$

Instead of simply “regular” and “inclined”, we consider 7 different galaxy types: ellipticals, and spirals of early (Sab) or late (Scd) types which are face-on (f, $0 < i < 40$), inclined (i, $40 < i < 75$), or edge-on (e, $75 < i < 90$). From our observations we know the approximate fractions of SNe II hosted by elliptical and spiral galaxies are $f_{HE} \sim 1/7$ and $f_{HS} \sim 6/7$. Based on the ratio between LOSS rates in field Sab and Scd spiral galaxies listed in Table 1, SNe II occur ~ 10 times more often in Scd than Sab spirals. We break f_{HS} down into components $f_{HSab} = 0.086$ and $f_{HScd} = 0.771$. Maltby et al. (2011) find the number fraction of cluster spirals which are face-on, inclined, and edge-on is 0.16, 0.66, and 0.18 respectively. The fractions of SN II hosts in each of our 7 considered galaxy types are: $f_{HE} = 0.143$, $f_{HSab(f)} = 0.014$, $f_{HSab(i)} = 0.057$, $f_{HSab(e)} = 0.015$, $f_{HScd(f)} = 0.0123$, $f_{HScd(i)} = 0.509$, and $f_{HScd(r)} = 0.139$.

Assuming all SNe II in face-on spirals are detected, we derive the fraction of SNe II detected in inclined and edge-on spirals from the rates presented in Table 3 of Li et al. (2011b). MENeACS and LOSS are both multi-epoch CCD SN surveys at low redshift, and it is reasonable to expect a similar inclination effect. LOSS did not target galaxies expected to produce extremely extinguished transients such as very dusty starburst galaxies, but neither does MENeACS since starbursts are not generally found in rich galaxy clusters. They consider the same 7 galaxy types as described above, and from their work we find $f_{SN_d(E)}=1.0$, $f_{SN_d(Sab(f))}=1.0$, $f_{SN_d(Sab(i))}=0.78$, $f_{SN_d(Sab(e))}=0.6$, $f_{SN_d(Sab(f))}=1.0$, $f_{SN_d(Sab(i))}=0.63$, $f_{SN_d(Sab(e))}=0.32$. This results in a MENeACS inclination correction factor of $C_{incl}=1.62$. By varying the component terms between their minimum and maximum values (e.g. the LOSS rates uncertainties), we estimate a $\sim 5\%$ uncertainty on C_{inc} and add this to our systematic uncertainties. Note that C_{inc} does not apply to our rates in red sequence galaxies.

B. APPROXIMATION TO A RATE INCORPORATING AN “EFFECTIVE” CONTROL TIME

The occurrence of unphysical rates can be avoided if, instead of choosing randomly from the SN II LF for each realization of the Monte Carlo, an effective control time is calculated using a sum over the components of the LF. In this method, Equation 1 becomes:

$$SNR_{II} = \frac{C_{inc}}{C_{spec}} \sum_i f_i \cdot \frac{N_{II,i}}{\sum_j \Delta t_{ij} M_j}, \quad (7)$$

where f_i is the weight of the i^{th} bin of the SN II LF, $N_{II,i}$ is the number of observed SNe II in the i^{th} bin, and Δt_{ij} is the control time for SN II from the i^{th} bin. This method is derived in the Appendix of Leaman et al. (2011), and is used by LOSS. Since MENeACS light curves are sparsely sampled, we do not have $N_{II,i}$, and this method is not appropriate for our dataset. We implement an approximation to this method by taking N_{II} outside the sum over i , and bringing $\sum_i f_i$ inside \sum_j to calculate an “effective” control time, integrated over the SN II LF, for every epoch. This style of rates calculation is more processor intensive, and for this trial we only run 100 realizations. The resulting rate for “All” galaxy types within R_{200} is $SNR_{II} = 0.023^{+0.030}_{-0.015}$ SNum, and no unphysical rates are encountered during the Monte Carlo. The upper uncertainties are smaller than those for our main method, $SNR_{II} = 0.026^{+0.075}_{-0.018}$, because the SN II LF does not contribute to the width of the rates distribution from the Monte Carlo realizations. We reiterate the subtle point that this is not appropriate for a survey such as MENeACS in which the observed LF, $N_{II,i}$, is not well characterized.